J Electroceram (2009) 22:136–144
DOI 10.1007/s10832-007-9367-0

The effects of aging and concentration on some interesting Sol-gel parameters: A feasibility study for PZT nanoparticles insertion on in-house prepared PAA matrices via electrophoresis

A. Suárez-Gómez · José. M. Saniger-Blesa · F. Calderón-Piñar

Received: 14 March 2007 / Accepted: 13 November 2007 / Published online: 1 December 2007

Abstract Sol-gel synthesis has been a very successful and efficient route for obtaining high quality ferroelectric/piezoelectric materials. Piezoelectric nanostructures, however, constitute a very recent field of research and special emphasis must be put on optimizing the packing of particles inside the nanoporous matrix in order to obtain nanomaterials with potential use on practical applications. In this work we study the influence of some critical sol features (aging time and concentration) on several interesting parameters when considering the electrophoretic insertion of Lead Titanate Zirconate (PZT) 53/47 nanoparticles in a Porous Anodic Alumina matrix. Our study focuses on pH, Zeta potential, Liquid Surface Tension, Mean Nanoparticles Size and Crystallization Routes. According to our results, and despite some previous reports, a successful electrophoretic deposition can be carried out on a wide range of concentrations and aging times.

A. Suárez-Gómez
Centro de Ultrasónica, ICIMAF,
Calle 15 #551 e/C y D Vedado,
Havana, 10400, Cuba

A. Suárez-Gómez (✉) · J. M. Saniger-Blesa
CCADET, UNAM, Ciudad Universitaria,
Circ. Exterior s/n, A.P. 70-186.,
Coyoacan, DF C.P. 04510, México
e-mail: amaury.sg@gmail.com

F. Calderón-Piñar
Facultad de Física/IMRE, San Lázaro y L,
Universidad de la Habana,
Havana, 10400, Cuba

Keywords Sol-gel · Ferroelectricity · Piezoelectricity · Propoxides · pH · Particle aggregation

1 Introduction

Sol-gel synthesis and processing of inorganic materials has proven to be a versatile, accurate and low cost procedure in order to guarantee appropriate mixing of reactants at molecular scale and good control over the stoichiometry of the desired compound. Powders, fibres, thin films, monoliths and nanowires have been obtained elsewhere by means of this method with controlled microstructure and its resulting influence on the final properties and performances of these materials [1, 2]. Far beyond these "final microstructure → properties" correlations, it is well known for the sol gel synthesis process that the stoichiometry, homogeneity, reactions conditions, purity and reactivity of the starting reactants play a decisive role on determining that desired final microstructure. As a result, several synthesis routes have been proposed for the same compound as well as different mixing conditions with numerous molar ratios among reactants. These apparent relativities, however, reinforce the flexible versatility and custom-made capabilities of the sol gel method.

Particularly, the Lead Titanate Zirconate ceramic system [$Pb(Zr_{1-x}Ti_x)O_3$; PZT $(1-x)/x$] is one of the most well known ferroelectric materials due to its high piezoelectric and dielectric response near the Morphotropic Phase Boundary (MPB), when $x \sim 0.48$, among other interesting features [3] that have been exploited in MEMs, FRAMs, acoustic sensors, ultrasound generation, etc. The sol gel synthesis of PZT has been receiving increasing interest for the last 20 years due to the limitations of the conventional

powders routes when dealing with molecular homogeneity [4, 5]; moreover, the interesting properties exhibited by low dimensional ferroelectric systems and the potential use of these ceramics in a plethora of nanodevices have risen this interest in recent years [6].

However, when treating the insertion of nanosized particles on nanoporous matrices via sol gel, several different approaches are followed by researchers [7]. Sometimes it is recommended an immediate insertion on the as-prepared solution and/or to synthesize sols with very low concentration without further explanation or systematical study [8–12]. The same can also be said for the particular case of the synthesis of PZT nanostructures [13, 14].

On a previous work [15] we studied two of the most popular alkoxide-based sol gel routes for synthesizing PZT, the butoxides- and the propoxides-based, resulting in better crystallization and homogeneity for the propoxides route under our experimental conditions. In this work we intend to study the feasibility of electrophoretic PZT nanoparticles insertion on the PAA matrices (<diameter$_{pore}$> ~ 70 nm) prepared by our workgroup [16]. We will concentrate on the influence of several sol gel parameters (pH, concentration, surface tension and aging) on the nanoparticles size and on the synthesis of PZT 53/47 nanopowders via the already chosen propoxides-based synthesis route.

2 A simple theoretical approach

According to the Diffuse Layer Theory for a simple electrolyte [17], it is well known that every charged colloidal spherical particle develops a potential ϕ fairly given by:

$$\phi \sim C\exp(-\kappa x) \sim C\exp\left(-x/\lambda_D\right), \tag{1}$$

being:

$$\kappa^2 = \left(1/\lambda_D\right)^2 = 2e^2 n_0/\varepsilon_M kT, \tag{2}$$

where e, n_0, ε_M, k and T are the electron charge, the bulk concentration of ions, the permittivity of the solution, the Boltzmann constant and the absolute temperature, respectively. λ_D is known as screening length or Debye length and the potential drop across the charge cloud at this distance is called the Zeta Potential (Z_P) and it is given, for weak potentials, by the following expression:

$$Z_P = q_0/\kappa\varepsilon_M, \tag{3}$$

where q_0 is the surface charge density.

When these particles, immersed in a viscous medium, move under the influence of a DC electric field, their associated velocity field must obey:

1. the Navier–Stokes equations:

$$\rho\frac{\partial\vec{u}}{\partial t} = \nabla\overleftrightarrow{\sigma} + \rho\vec{f} = -\nabla p + \eta\nabla^2\vec{u} + \rho\vec{f}, \tag{4}$$

and

2. the mass conservation law:

$$\frac{\partial\rho}{\partial t} = -\nabla\left(\rho\vec{u}\right). \tag{5}$$

Assuming the body forces are given by the component $E_{\|}$ of the electric field vector along a charged surface, we have:

$$\vec{f} = \rho_e E_{\|}\hat{z}, \tag{6}$$

where ρ_e is the particle mass-charge electric density. Solving for spherical, and non-interacting, particles with radius a, velocity can be written as:

$$\vec{u} = \left(q_0/6\pi\eta a\right)E\,\hat{z}, \tag{7}$$

implying that electrophoretic mobility μ can be expressed as:

$$\mu = q_0/6\pi\eta a. \tag{8}$$

In the Hückel–Onsager approximation, very small particles are immersed in a low dielectric constant medium thus implying $\kappa a \ll 1$. In this case, the electrophoretic mobility is given by:

$$\mu = 2\varepsilon_M Z_P/3\eta. \tag{9}$$

When these moving charged particles deposit on an electrode they will imply a deposited weight (w) per unit area of electrode. According to a simple model by Ishihara [18], Chen and Liu [19], this extra weight can be calculated by:

$$w = \frac{2\varepsilon_M Z_P}{3\eta}C\left(\frac{E}{L}\right)t = \mu C\left(\frac{E}{L}\right)t, \tag{10}$$

where C, L and t are the concentration of the particles, the distance between the electrodes and the deposition time, respectively.

According to this result, numerous factors influence the electrophoretic deposition (EPD) of particles on a given

electrode: Zeta potential, concentration, applied potential, deposition time, medium viscosity (or surface tension) and permittivity, particles size, etc. A good review about the factors influencing the EPD process, especially for films synthesis, can be found on [20].

When synthesizing nanostructures inserted on PAA matrices through EPD, the picture is more complicated considering the small pore diameter and, as pointed out by Martin et al. [21–23], the possible interactions between anionic or cationic defects located at the pore wall and the moving charged particle.

With this work we plan to start a study aimed at the optimization of the synthesis process of PZT 53/47 nanostructures embedded on in-house prepared PAA matrices. Here we will focus on the influence of some easily modifiable sol gel parameters (pH, concentration, zeta potential, surface tension and aging) on the nanoparticles size and on the synthesis of PZT 53/47 nanopowders via the propoxides-based synthesis route.

3 PZT sol synthesis

The followed synthesis route is depicted in Fig. 1. Starting reagents for the sol gel PZT solution were: (1) lead (II) acetate trihydrate ($Pb(OAc)_2{\cdot}3H_2O$, Mallinckrodt Baker, Inc., 99.8% pure), (2) glacial acetic acid (HOAc, Mallinckrodt Baker, Inc., 99.7% pure), (3) zirconium (IV) propoxide ($Zr(OPr)_4$, Sigma-Aldrich Co., 70 wt. % in 1-propanol), (4) titanium (IV) propoxide ($Ti(O^iPr)_4$, Sigma-Aldrich Co., 97% pure). (5) acetylacetone (AcacOH, Sigma-Aldrich Co., 99% pure) and (6) 2-methoxyethanol (2-MOE, Mallinckrodt Baker, Inc., 100% pure).

First, lead acetate was dissolved in acetic acid with a 1:3 molar ratio while stirred and refluxed at 115°C during 3 hours for water removal and homogeneity purposes. After this step, a thick transparent solution was obtained which will be referred hereafter as Solution A.

On a separate process, stoichiometric amounts of zirconium and titanium alkoxides were mixed with acetylacetone on a 1:3.06 molar ratio in order to avoid fast hydrolysis of reactants. This mixture was stirred and refluxed at 90 °C during 4 h forming a clear yellow solution referred hereafter as Solution B. In this step, two different chelated metal complexes are formed along with the residual alcohol: $Zr(Acac)_4$ and $Ti(OPr)_2(Acac)_2$. In both complexes the central atom attains its maximum coordination number and, therefore, these are the most stable configurations for each metal. Anyway, some other reports [24–26] account for the formation of several 'incomplete' chelated complexes under different mixing conditions and this fact must be taken into consideration when designing/choosing the experimental route.

Afterwards, Solutions A and B were then mixed together as appropriate amounts of solvent (2-MOE) were slowly added for controlling pH, viscosity and liquid surface tension. In this step, the dissolved lead acetate complex can react with 2-MOE forming a very stable acetate-methoxyethoxy lead complex [1, 24] that, along with the chelated metal complexes already formed, turn this final solution in an hydrophobic sol, poorly hydrolysable and, therefore, very stable long after shelving for 3–4 months without particles sedimentation.

Right after mixing Solutions A and B, a light yellow solution was obtained after stirring for 24 h at room temperature. For the purposes of this study, the PZT concentration on the final solutions was varied from 0.37 to 0.05 M. Portions of the resulting solutions were heated at 100 °C until dried and thermally treated in order to analyze the phase evolution from the amorphous PZT sol gel network to the expected final perovskite structure.

4 Liquid surface tension

Liquid Surface Tension (σ) of sols was measured as a function of the aging time according to the Du Noüy Standard Ring method using the Huh & Mason correlation method. From these results, no visible dependence could be inferred (see Table 1): after 45 days on shelf, sols apparently still tend to retain the mechanical properties of solvent (σ_{2-MOE}=30.05 mN/m) at a macroscopic level.

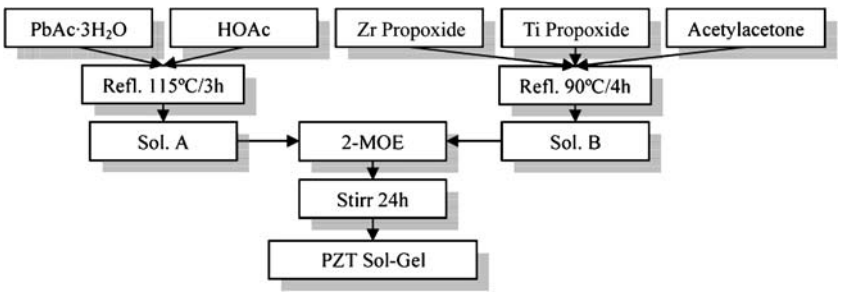

Fig. 1 Flow chart depicting the basic experimental procedure followed in order to obtain the 0.4 M PZT 53/47 sol gel

Table 1 Surface tension (σ) of as prepared sols (σ_0) and sols after 45 days of shelving (σ_{45}) for every studied concentration.

Sol concentration (M)	σ_0 (mN/m) $<\sigma_0>=30.23$	σ_{45} (mN/m) $<\sigma_{45}>=29.73$
0.37	29.88	29.32
0.35	30.01	29.66
0.31	29.84	29.5
0.27	29.87	29.71
0.20	30.56	29.17
0.15	31.12	30.04
0.10	30.47	30.18
0.05	30.12	30.23

Mean values for each aging time are also reported. All samples were measured at 20 °C.

Bulk surface tension, in this case, does not seem to be a parameter affected by the change in concentration or aging time of the PZT sols.

5 pH and zeta potential

On the other hand, the acidity/basicity of the solutions clearly shows a tendency with both sols concentration and aging time. Figure 2 shows the measured pH for the studied sols at several aging steps; semi-log fittings for the pH vs. Concentration behaviors are also drawn.

As a general tendency, sols pH dependency with aging time can be divided in three stages: (1) pH increases notably in the first days after which (2) it decreases to values somehow close to the initial ones. In this moment, (3) pH starts to rise again but with a slower time gradient than on stage (1). At this point we must stress that,

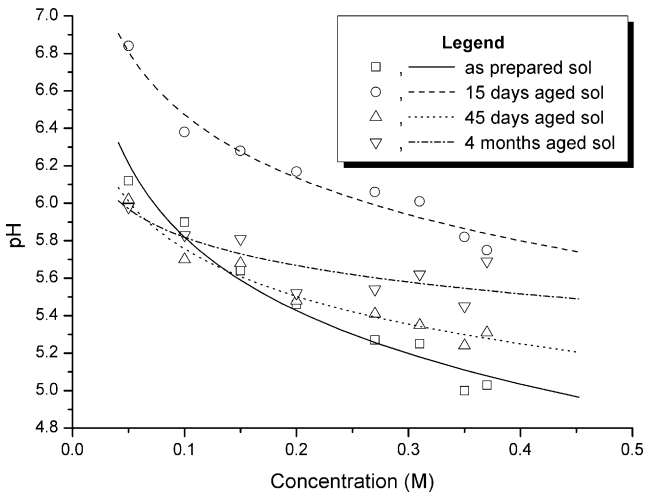

Fig. 2 pH vs. concentration dependencies for all the samples under study measured at different time intervals. Semi-log fittings are also drawn

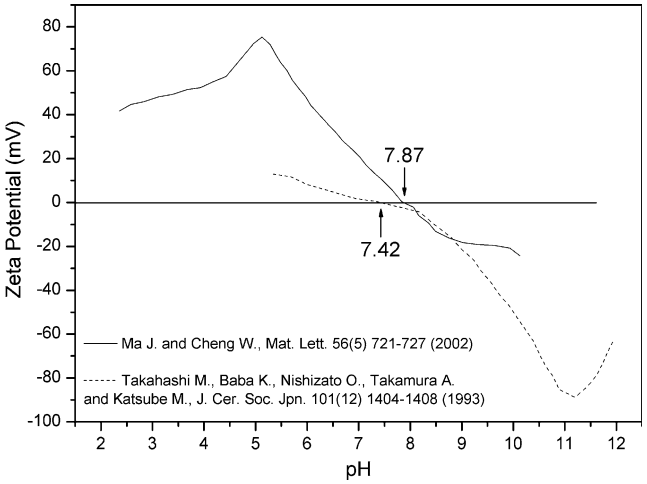

Fig. 3 Available Z_P vs. pH data for the PZT system taken from [27] and [28]. Differences between both reports are highlighted. According to the results shown in Fig. 1, our colloidal particles, even after aging for 4 months, are positively charged

according to the available data [27, 28] (see Fig. 3), the reported pH values are well below the isoelectric points commonly accepted in the literature for the PZT system and, therefore, charged particles in all the studied colloids are positively charged. Even though highlighted, the analysis of discrepancies between both reports is out of the scope of this work.

In our opinion, for the understanding of the pH vs. aging time behavior, we have to take into account the coexistence of different competitive processes right after sols were prepared. In this way, a qualitative description could be done as follows [1]: (1) Remnant unreacted acetic acid evaporates during the first days implying an increment on the basicity of sols. At this point, (2) particles are less positively charged and are able to aggregate via oxolation reactions followed by deprotonation of the oligomeric species and, as a consequence, acidity is increased. It is also possible that some small amount of alcohol is formed by means of residual alkoxy radical protonation and thus implying a more acid environment as seen in Fig. 2. The number of polyanions per aggregate chain must be limited, however, by the high chemical stability of the chelated metal complexes and that is why the deprotonation process does not imply polymerization and/or gelation as it has been reported for more hydrophilic sols. Shortly after deprotonation rate vanishes, (3) it is possible for the residual alcohols to evaporate as solutions age thus allowing pH to rise slowly, as seen in Fig. 2 for the more aged solutions.

At this scenario, however, hydrolysis is not expected due to (a) the complete chelation of the metal complexes, (b) to the short lengths of the already formed polymeric chains and, therefore, (c) to the small amount of alcohol that could be formed afterwards. After 4 months of aging, no noticeable

change in pH values was detected. Moreover, the stability of these solutions could be eye-inspected by verifying neither the absence of sedimentation nor precipitation of single particles or aggregates after almost 1 year of stocking.

6 Particles size

A few drops of the synthesized sols were deposited on copper grids and evaporated afterwards for Transmission Electron Microscopy (TEM) observation using a JEOL JEM-1200 EX microscope.

Two effects influencing particles size were tracked with this technique: sol aging and sol concentration.

Figures 4(a) and (c) show low resolution TEM images for two concentrations (0.37 and 0.35 M, respectively) being on stock for 1 month after synthesis. On the right column of the picture, Fig. 4(b) and (d) show TEM images for the same solutions after 4 months. A similar behavior was observed for the rest of our samples.

Electron diffraction patterns were also obtained and the typical series of concentric rings corresponding to a polycrystalline material are also shown on each photograph. In all figures, zones without particles aggregates correspond to the previously evaporated solvent 2-MOE.

As can be seen in this case, as sols are aged the distribution of particles size seems to be more uniform and with a mean value slightly lower than on fresher solutions. This fact, along with the observed small particle size (~1–10 nm), validates

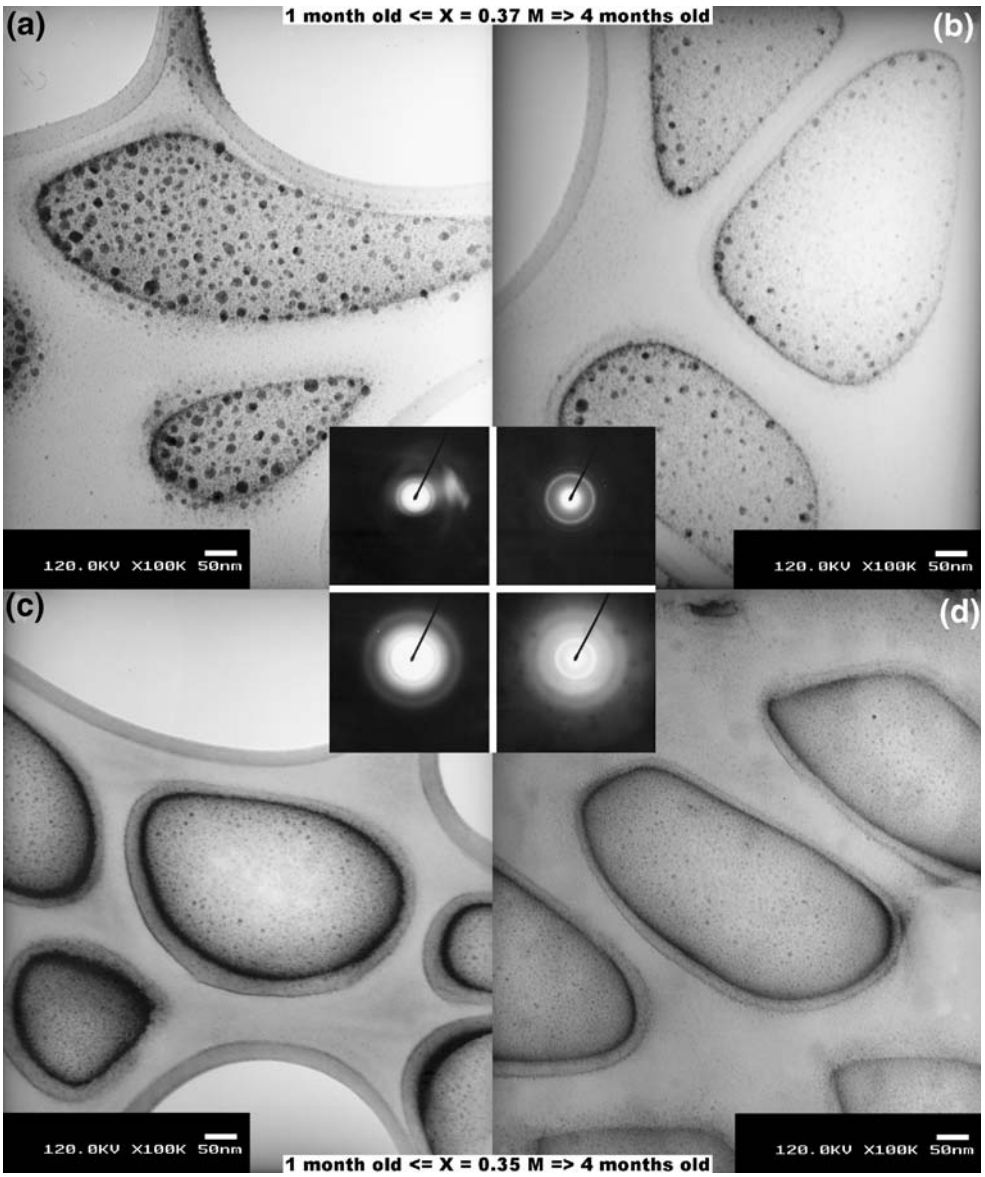

Fig. 4 Effects of solutions aging on particles size as illustrated by TEM photographs to the 0.37 M and 0.35 M sols. The figure shows the 0.37 M sol aged for (**a**) 1 and (**b**) 4 months and the 0.35 M sol identically aged for (**c**) 1 and (**d**) 4 months. Similar behaviors were exhibited by all the concentrations under study. Some concentration effects are clearly seen

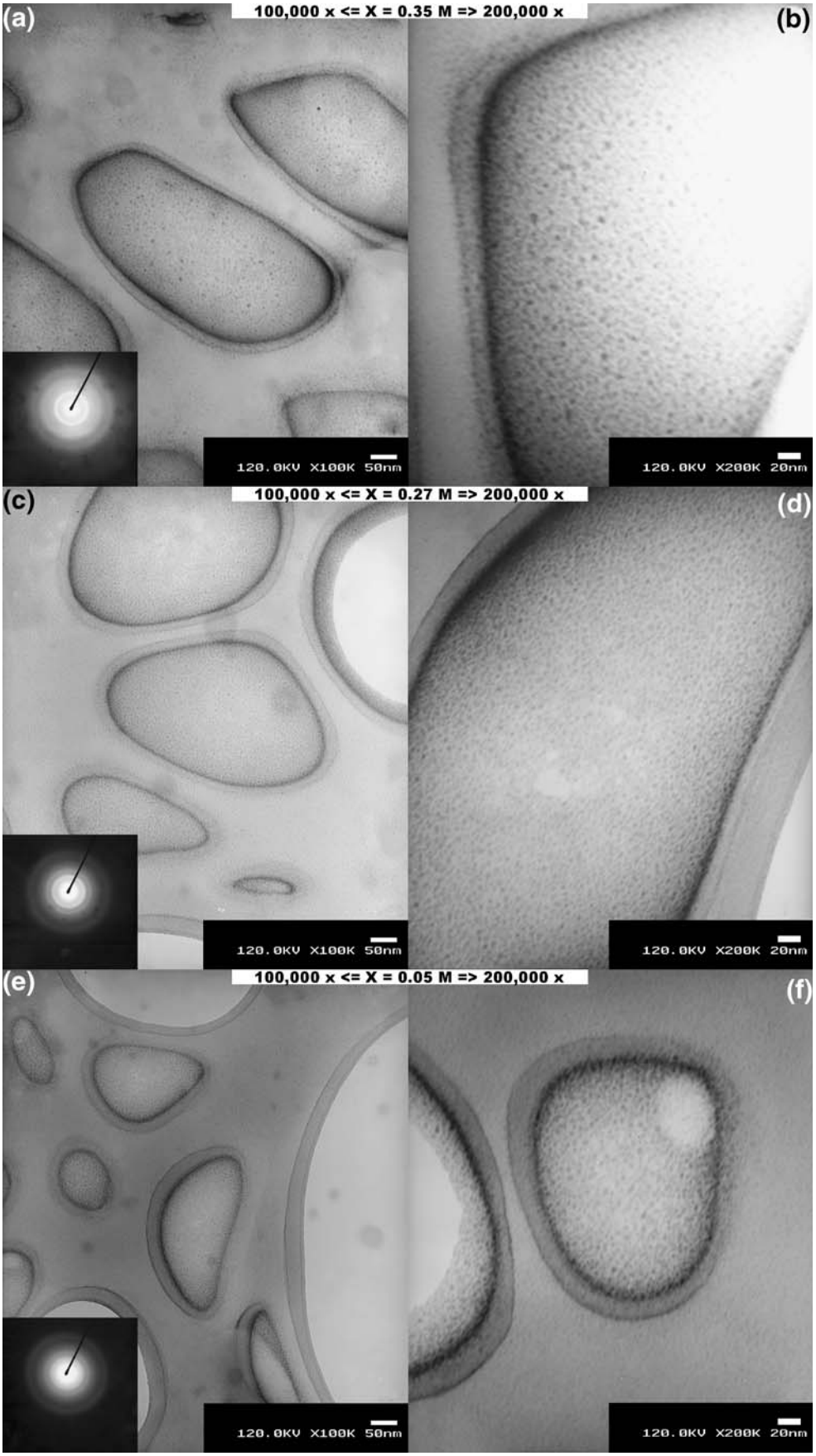

Fig. 5 Effects of concentration on particles size as illustrated by TEM photographs to the 0.35, 0.27 and 0.05 M sols. The figure shows two different magnifications for each concentration: (**a**), (**c**), (**e**) × 100,000 and (**b**), (**d**), (**f**) × 200,000. According to these results, particle size tends to stabilize when concentration is lowered and being about 1–2 nm for almost every studied concentration

somehow what was previously said about the inferred short lengths of the polymeric chains and about the stability of the completely chelated metallic complex. As time passes, no hydrolysis is detected in our samples and polymeric chains tend to stabilize the solutions on a very noticeable way.

The figure also shows how concentration drastically influences the particles size, specially for the higher concentrations under study. For lower concentrations, as seen in Fig. 5, the influence is not so strong.

Obviously, dried aggregates are smaller with lower concentrations (and that is clearly depicted in the figures) but nanoparticles size seems to reach a limit size mainly fixed by pH and coordination of the metallic oxo-acetylacetonates with the acetate-methoxyethoxy lead complex.

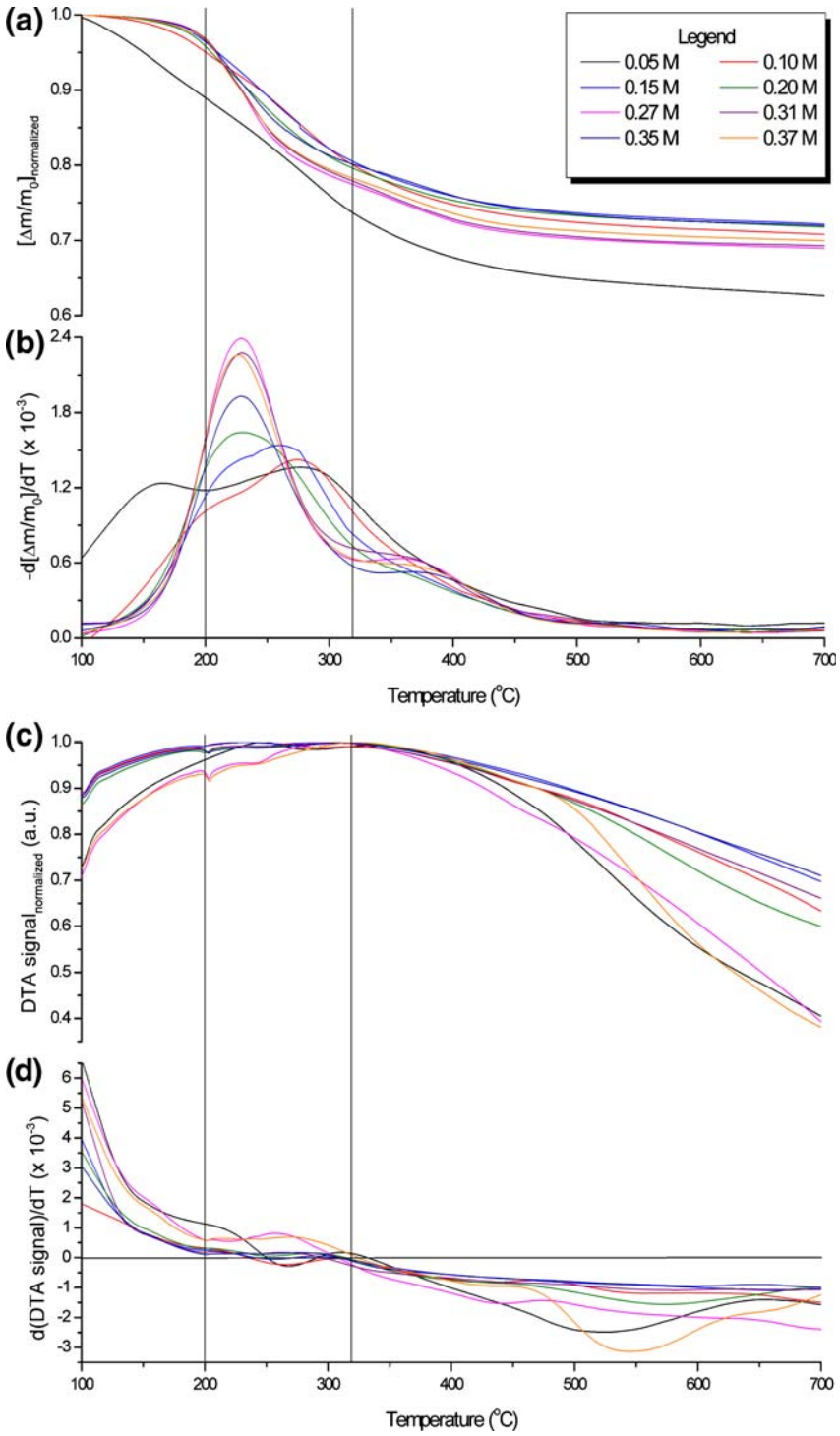

Fig. 6 (**a**) TGA and (**c**) DTA signals for sol-derived dried powders and for every studied concentration. The slight differences among those measurements are better seen when analyzing their derivatives (**b**) and (**d**), respectively, which are graphed below each family of curves. The three main stages at which decomposition and crystallization occur are highlighted with vertical lines

In the right column of Fig. 5 we show magnified TEM images (× 200,000) of the same sols shown in the left (× 100,000). As getting closer to the instrument magnification limit (~ × 500,000 or ~0.2 nm) it was clear that mean particles size is around 1 nm even though acceptable focusing was hard to achieve.

7 Crystallization

For thermogravimetric/calorimetric analysis, a TA Instruments Q600 SDT analyzer was used in dynamic rate mode. Heating rates were constrained to 5 °C/min from an initial temperature of 100 °C to a final temperature of 700 °C. The furnace purge was nitrogen using flow rates of 100 mL/min.

The thermal decomposition of the as-dried PZT sols under study was monitored by TGA and DTA analysis and both normalized data are shown in Fig. 6; the derivatives of every recorded signal are also shown in order to highlight the slight differences among them.

Generally speaking, it can be seen that three main stages could be identified and are highlighted by vertical lines on each graph: (1) a first reaction until 200 °C associated with the evaporation of residual organic solvents, (2) subsequent mass losses when heating to about 320 °C accompanied by some exothermic peaks and evolution of CO_2 and H_2O attributed to oxidation of organic species (alkoxides, acetates, acetylacetonates).

These various exothermic steps have also been reported for the chelated acetylacetone PZT sol gel route and have been identified with the decomposition product of acetate groups [29, 30]. Finally, (3) when heating up to 700 °C, mass losses are registered accompanied by another exothermic peak at about 350 °C associated with the decomposition of carbonaceous species. Further heating reveals a rather weak exothermic transformation in the 500–550 °C temperature range without significant mass losses indicating a possible phase transformation that, in our case, can be attributed to the pyrocholore-perovskite (Pyr-Per) phase transition [15].

The influence of concentration on the crystallization route is almost negligible due to the slight differences observed when determining the Pyr-Per phase transition (Fig. 5(c) and (d)). In the first stages, however, the organic decomposition occurs in two steps transforming into one single step as concentration gets higher (Fig. 5(a) and (b)). Anyway, for PZT synthesis purposes, these first stages on decomposition/crystallization do not posses a particular interest.

8 Feasibility of PZT nanotubes synthesis

At this point, summarizing all our previous results, we might ask ourselves about the possibility of PZT nanotubes electrophoretic synthesis by using in-house prepared PAA matrices (<diameter$_{pore}$> ~ 70 nm) as the one showed on the AFM images of Fig. 7(a) and (b) [16].

According to what we have seen until now, particles are small enough to fill the pores, especially for not so high sol

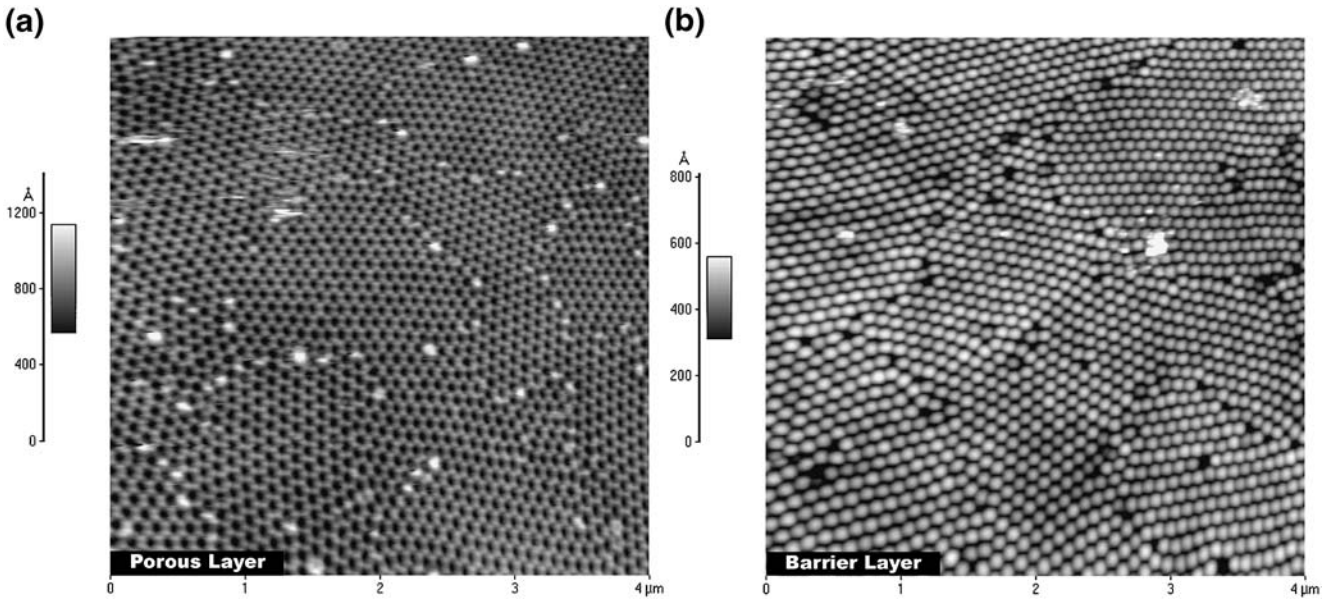

Fig. 7 Porous Anodic Alumina (PAA) matrix prepared by our workgroup as reported in 0. AFM image shows (**a**) the porous layer [*top view*] and (**b**) the barrier layer [*bottom view*] of the template. Mean pore diameter is about 70 nm, apparently feasible for the insertion of nanoparticles shown in Figs. 4 and 5. For electrophoresis purposes, the barrier layer has to be removed

concentrations. Moreover, particles are always positively charged, suitable for anodic deposition, and sols have similar surface tension regardless of concentration or shelving time.

If we take into account the simple reasoning that led us to Eqs. 9 and 10, an optimum DC electric field (E)—Deposition time (t) relationship must exist for every single concentration under study in order to achieve an optimum pore filling via electrophoresis. Needless to say, an optimum pore filling will imply an optimum sintered density after heat treatment and practical applications for these nanotubes arrays as mechanical or electrical sensors will be enhanced.

A study for determining the optimum conditions for PZT nanotubes synthesis is currently being carried out.

9 Conclusions

In this work we studied the influence of sol concentration and aging on pH, Zeta potential, liquid surface tension, particles size and crystallization routes for several solutions of PZT 53/47 propoxy-based sols. These solutions, regardless of the sols concentration, behave mechanically just like the solvent, 2-MOE in our case, and, according to the pH measurements and to the available Zeta potential reports, colloidal particles remain positively charged even after 4 months of stocking.

Apparently, particles size tends to be smaller and more homogeneously distributed as aging time increases. In all cases, particles are about 1–2 nm in size and we did not find a drastic concentration dependence of this crucial parameter even though concentrations below 0.35 M showed a more homogeneous size distribution. Unfortunately, but also helpfully, in-situ colloidal particle size measurements were not possible to obtain due to their small size. On the other hand, crystallization routes do not feature any significant difference among the studied solutions and the important Pyr-Per phase transition takes place between 500 and 550 °C for every studied concentration.

Our results showed that neither aging nor concentration appear to be critical issues when considering nanoparticles insertion on in-house prepared PAA matrices, particularly for concentrations below 0.35 M. The handicaps of concentration and shelving time, indicated by some authors, seem to be avoided, in our humble opinion, by synthesizing a completely chelated metallic oxo-complex when reacting with acetylacetone in the initial reactions.

Acknowledgements Authors would like to gratefully acknowledge the support given by Quím. A. Y. Ordóñez Medrano, Quím. E. Fregoso Israel, M. en C. J. Guzmán Mendoza and Téc. C. Flores Morales from IIM, UNAM. We also appreciate the kind help provided by Dr. R. Zanella Specia, M. en C. J. Guadalupe Bañuelos, M. en C. J. O. Flores Flores and M. en C. M. E. Mata Zamora, from CCADET, UNAM. A. Suárez-Gómez thanks the financial support provided through CLAF-ICTP-TWAS and UNAM-DGEP scholarships.

References

1. C.J. Brinker, G.W. Scherer, *Sol Gel Science: The Physics and Chemistry of Sol Gel Processing* (Academic, San Diego, 1990)
2. L.C. Klein (Ed.), *Sol Gel Technology for Thin Films, Fibers, Preforms, Electronics, and Specialty Shapes* (Noyes, New Jersey, 1988)
3. B. Jaffe, W.R. Cook, H. Jaffe, *Piezoelectric Ceramics* (Academic, New York, 1971)
4. B.A. Tuttle, R.W. Schwartz, Mater. Res. Bull. **21**(6), 49 (1996)
5. R.W. Schwartz, Chem. Mater. **9**, 2325 (1997)
6. Z.L. Wang, Materials Today **10**(5), 20 (2007)
7. K. Shantha Shankar, A.K. Raychaudhuri, Mater. Sci. Eng., C **25**, 738 (2005)
8. J.J. Urban, W.S. Yun, Q. Gu, H. Park, J. Am. Chem. Soc. **124**(7), 1186 (2002)
9. T. Valdés-Solís, G. Marbán, A.B. Fuertes, Chem. Mater. **17**(8), 1919 (2005)
10. G. Mu, S. Yang, J. Li, M. Gu, J. Mater. Process. Technol. **182**, 382 (2007)
11. E.D. Mishina, K.A. Vorotilov, V.A. Vasiliév, A.S. Sigov, N. Ohta, S. Nakabayashi, J. Exp. Theor. Phys. **95**(3), 502 (2002)
12. M. Steinhart, Z. Jia, A.K. Schaper, R.B. Wehrspohn, U. Gösele, J. H. Wendorff, Adv. Mater. **15**(9), 706 (2003)
13. S.J. Limmer, S. Seraji, Y. Wu, T.P. Chou, C. Nguyen, G. Cao, Adv. Funct. Mater. **12**(1), 59 (2002)
14. S.J. Limmer, S. Seraji, M.J. Forbess, Y. Wu, T.P. Chou, C. Nguyen, G. Cao, Adv. Mater. **13**(16), 1269 (2001)
15. A. Suárez-Gómez, R. Sato-Berrú, R.A. Toscano, J.M. Saniger-Blesa, F. Calderón-Piñar, J. Alloys Compd. (2006), DOI 10.1016/j.jallcom.2006.10.143
16. M.E. Mata-Zamora, J.M. Saniger, Rev. Mex. Fís. **51**(5), 502 (2005)
17. T.M. Squires, S.R. Quake, Rev. Mod. Phys. **77**(3), 977 (2005)
18. T. Ishihara, K. Shimise, T. Kudo, H. Nishiguchi, T. Akbay, Y. Takita, J. Am. Ceram. Soc. **83**(8), 1921 (2000)
19. F. Chen, M. Liu, J. Eur. Ceram. Soc. **21**, 127 (2001)
20. L. Besra, M. Liu, Prog. Mater. Sci. **52**, 1 (2007)
21. B.B. Lakshmi, P.K. Dorhout, Ch.R. Martin, Chem. Mater. **9**, 857 (1997)
22. Ch.R. Martin, Chem. Mater. **8**, 1739 (1996)
23. B.B. Lakshmi, Ch.J. Patrissi, Ch.R. Martin, Chem. Mater. **9**, 2544 (1997)
24. J. Livage, M. Henry, C. Sanchez, Prog. Solid State Chem. **18**, 259 (1988)
25. M. Sedlar, M. Sayer, J. Sol Gel Sci. Technol. **5**, 27 (1995)
26. U. Schubert, N. Husing, A. Lorenz, Chem. Mater. **7**, 2010 (1995)
27. J. Ma, W. Cheng, Mater. Lett. **56**(5), 721 (2002)
28. M. Takahashi, K. Baba, O. Nishizato, A. Takamura, M. Katsube, J. Ceram. Soc. Jpn. **101**(12), 1404 (1993)
29. B. Malic, M. Kosec, I. Arcon, A. Kodre, J. Eur. Ceram. Soc. **25**, 2241 (2005)
30. R. Caruso, O. de Sanctis, A. Frattini, C. Steren, R. Gil, Surf. Coat. Technol. **31**, 44 (1999)